

VJT : A Video Transformer on Joint Tasks of Deblurring, Low-light Enhancement and Denoising

Yuxiang Hui¹, Yang Liu², Yaofang Liu³ Fan Jia¹
Jinshan Pan⁴ Raymond Chan³ Tiejong Zeng¹

¹The Chinese University of Hong Kong, ²National University of Defense Technology,
³City University of Hong Kong, ⁴Nanjing University of Science and Technology

Abstract

Video restoration task aims to recover high-quality videos from low-quality observations. This contains various important sub-tasks, such as video denoising, deblurring and low-light enhancement, since video often faces different types of degradation, such as blur, low light, and noise. Even worse, these kinds of degradation could happen simultaneously when taking videos in extreme environments. This poses significant challenges if one wants to remove these artifacts at the same time. In this paper, to the best of our knowledge, we are the first to propose an efficient end-to-end video transformer approach for the joint task of video deblurring, low-light enhancement, and denoising. This work builds a novel multi-tier transformer where each tier uses a different level of degraded video as a target to learn the features of video effectively. Moreover, we carefully design a new tier-to-tier feature fusion scheme to learn video features incrementally and accelerate the training process with a suitable adaptive weighting scheme. We also provide a new Multiscene-Lowlight-Blur-Noise (MLBN) dataset, which is generated according to the characteristics of the joint task based on the RealBlur dataset and YouTube videos to simulate realistic scenes as far as possible. We have conducted extensive experiments, compared with many previous state-of-the-art methods, to show the effectiveness of our approach clearly.

Introduction

Image and video restoration, which aim to provide high-quality videos, have been long-standing important tasks in computer vision. Most of the existing approaches to image and video restoration problems design models and datasets for a specific task, such as video deblurring (Wang et al. 2019c; Zhong et al. 2020; Pan, Bai, and Tang 2020; Son et al. 2021; Zhong, Zheng, and Sato 2021; Ji and Yao 2022; Liang et al. 2022a; Lin et al. 2022), denoising (Maggioni et al. 2012; Arias and Morel 2018; Chen, Song, and Yang 2016; Qi et al. 2022; Tassano, Delon, and Veit 2019), low light enhancement (Guo, Li, and Ling 2016; Fu et al. 2015; Lore, Akintayo, and Sarkar 2017; Lv et al. 2018; Peng et al. 2022; Zhang et al. 2021; Xu et al. 2020; Guo et al. 2020; Triantafyllidou et al. 2020), deraining (Yue et al. 2021; Yang, Liu, and Feng 2019; Li et al. 2018b; Wang et al. 2019b; Zhang et al. 2022). However, in the real world, many conditions that lead to low-quality video often occur simultane-

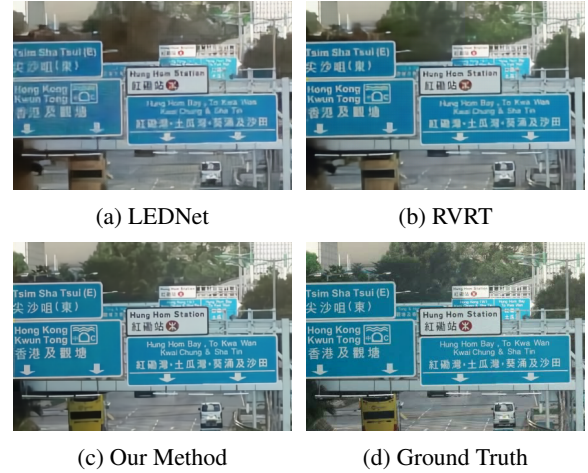


Figure 1: Restoration results on a part of a frame from a daytime outdoor scene of our dataset. Our method simultaneously removes blur, enhances low light and eliminates noise. Compared to three recent methods retrained on our MLBN dataset, our method improves image quality in terms of object detail.

ously. For instance, we can have low light, blur, and noise from relatively long exposures at the same time when we take videos at night. This raises the urgent need to handle joint recovery tasks on images and videos.

Note that video deblurring, low-light enhancement, and denoising are among the most critical and challenging tasks in the field of video restoration. Many previous recurrent methods have proven effective in solving video recovery problems due to the sequential character of videos. In particular, several transformer models (Girdhar et al. 2018; Liu et al. 2021b; Liang et al. 2022a,b; Bertasius, Wang, and Torresani 2021; Arnab et al. 2021) have performed exceptionally well for these tasks separately in recent years.

As existing deblurring methods, light enhancement and denoising methods can deal with each problem individually, one can simply combine these methods sequentially for the joint task. However, this direct combination may not achieve the best results for low quality images and videos suffered from blurring, low visibility and heavy noise simultane-

ously. The reason for this unsatisfactory result is clear. Indeed, a system processing low-quality videos to high-quality videos sequentially will lose some valuable information step by step and may revoke unknown noise and artifacts for the coming individual task. The joint task can better utilise all the valuable information for video restoration.

In this regard, it is natural for us to consider the joint task of video deblurring, low-light enhancement and denoising simultaneously to get the best restoration results. Immediately, we need to handle two critical issues: a suitable dataset for the joint task and a leading joint video restoration method. Our paper will address both issues effectively.

Indeed, the first aim of our work is to provide a suitable dataset for the joint task of deblurring, lowlight enhancement and denoising. This Multi-scenes Lowligh-Blur-Noise (MLBN) dataset contains 195 scenes, covering indoor, nighttime outdoor and daytime street scenes, which are often involved in video recording. We propose a data generation progress to obtain realistic low-light blurry videos with noise. For the blurring part, we use the method in (Nah, Kim, and Lee 2016) to gain the corresponding blurry and clear frames from the high frame rate videos. As for the low-light part, we design an inverse LIME-based algorithm, considering the Retinex model LIME(Guo, Li, and Ling 2016). In addition, we have made different degrees of degradation for both the illumination and reflectance components, which will give more realistic results than simply using the inverse LIME algorithm. Finally, we employ the CycleISP algorithm to synthesise noise.

Based on our progress in data generation for the MLBN dataset, videos of different stages of degradation are produced. Inspired by this, our second aim is to propose a leading joint video restoration method. Indeed, we design a multi-tier video transformer framework whereby each tier uses ground truth videos with different degradation levels as targets. A feature fusion method is used between tiers to transfer the features learned in the previous tier to the next one. This allows the network to step up the learning of features to three subtasks, resulting in a better reconstruction. In addition, we employ an adaptive weight scheme to cope with the multiple loss functions of the joint task. It allows the different loss functions to reach the same energy level, thus making the training process more efficient. This accelerates the training and enables higher results at each stage of the progressive joint task.

In summary, the main contributions of our paper are as follows:

- We propose the VJT, a **Multi-tier Video Transformer** that can get differentiated features from three progressive tasks. We use the **Feature Fusion** between tiers to make the structure more efficient. We also use an **Adaptive Weight Scheme** to balance the magnitude of different losses to speed up training and achieve better results.
- We are pioneering researchers to address the integrated challenges of **Joint Video Restoration** by using our VJT.
- We propose a new data generation progress that balances the visibility, information density and noise intensity well in low-light videos to approximate real scenes

closely enough. We have generated a new **Multi-scene Lowligh-Blur-Noise (MLBN) Dataset** for our joint task.

Related Work

Video Transformer.

Transformer-based models (Vaswani et al. 2017; Dosovitskiy et al. 2021; Carion et al. 2020; Liu et al. 2021a, 2022, 2021b; Xie et al. 2021) have shown effective results for various vision tasks. The Swin-Transformer proposed by Liu (Liu et al. 2021a, 2022, 2021b; Xie et al. 2021) has performed very well in multiple areas such as objection detection, semantic segmentation, and action classification. Compared to image tasks, video transformers need to consider one more temporal attention, and several works are excellent on video tasks(Girdhar et al. 2018; Liu et al. 2021b; Liang et al. 2022a,b; Bertasius, Wang, and Torresani 2021; Arnab et al. 2021). Liang (Liang et al. 2022a) proposed a Video Restoration Transformer that combines space attention and temporal attention based on Swin Transformer. Then they suggested RVRT (Liang et al. 2022b), which uses a globally recurrent framework and locally temporal attention module. Bertasius (Bertasius, Wang, and Torresani 2021) compared different paradigms that unify temporal and spatial attention.

Deblurring.

Traditional methods (Li et al. 2010; Kim and Lee 2015) are based on image and video priors and assumptions. In recent years, as computing power has increased, deep learning methods have begun to be applied on a large scale (Wulff and Black 2014; Su et al. 2017; Gong et al. 2017; Hyun Kim et al. 2017; Wang et al. 2019c; Zhong et al. 2020; Pan, Bai, and Tang 2020; Ji and Yao 2022; Son et al. 2021; Zhong, Zheng, and Sato 2021). Most of them use CNN, RNN-based methods. Ji (Ji and Yao 2022) designed a multi-scale bidirectional recurrent method using a memory-based feature aggregation. In the last two years, with the popularity of Transformer architecture, there are several articles(Lin et al. 2022; Liang et al. 2022a,b; Zhang, Xie, and Yao 2022; Zhong et al. 2020) using a transformer for video deblurring. Wang (Wang et al. 2019c) proposed a pyramid, cascading and deformable convolution module for alignment and a TSA module for feature fusion. They were early adopter of the attention model for deblurring. Zhang (Zhang, Xie, and Yao 2022) proposed a spatio-temporal deformable attention module for video deblurring. Lin (Lin et al. 2022) customised a flow-guided sparse window-based multi-head self-attention module for video deblurring.

Low-light Enhancement.

Traditional low light enhancement methods include Retinex-based (Guo, Li, and Ling 2016; Fu et al. 2015; Hao et al. 2019; Park et al. 2017) and histogram-based methods (Ibrahim and Kong 2007; Abdullah-Al-Wadud et al. 2007). The method based on the Retinex model is used more often; it generally decomposes the low-light image into illumination and reflection components by some regularisation or a

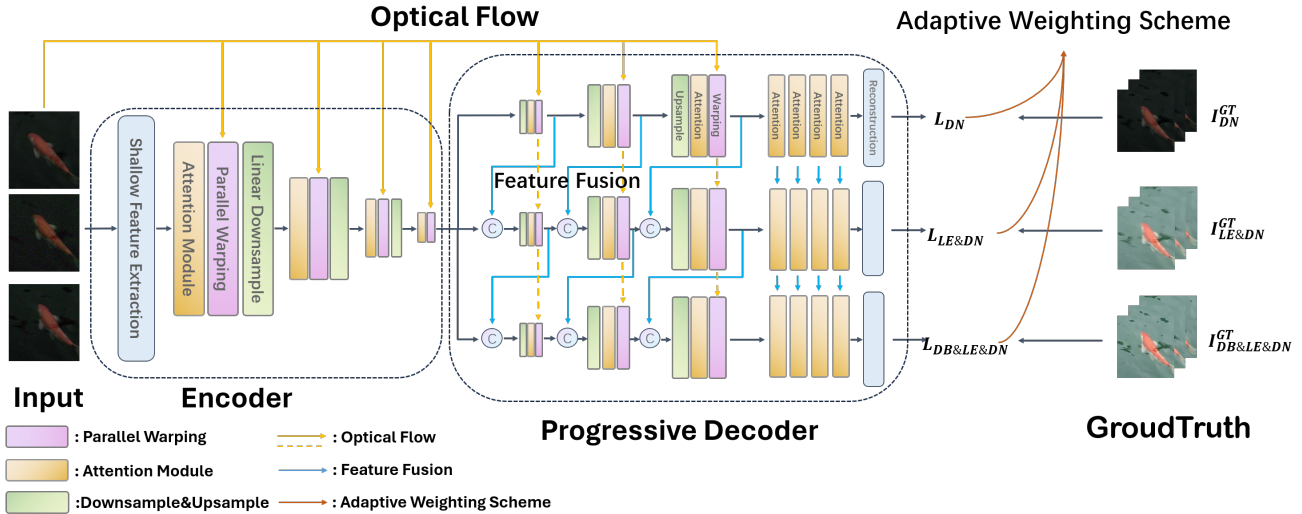


Figure 2: An illustration of the proposed VJT. It contains a single tier Encoder and a Multi-tier Decoder. There are multiple scales Attention-Warping modules in both the encoder and decoder. A shallow feature extraction module begins, while four attention and a reconstruction module are at the end. Each tier obtains a video with a different level of restoration. Feature fusion modules between tiers can transfer features for progressive joint tasks. The skip connections have been omitted for clarity.

prior condition and then enhances the illumination component to obtain the normal light image. LIME is a representative of Retinex models, which proposes two algorithms for accelerating the calculation of illumination maps. The deep learning-based approach also achieves strong results in image and video low-light enhancement (Lore, Akintayo, and Sarkar 2017; Lv et al. 2018; Peng et al. 2022; Zhang et al. 2021; Xu et al. 2020; Guo et al. 2020; Triantafyllidou et al. 2020). (Lv et al. 2018) extracted features through a feature extraction module, an enhancement module, and a fusion module. There is also a group of models that combine traditional Retinex methods with deep networks (Wei et al. 2018; Yang et al. 2021; Li et al. 2018a; Wang et al. 2019a; Zhang, Zhang, and Guo 2019). (Wei et al. 2018) used a decom-net to divide the image into reflective and illuminated components and an enhancement-net for low light enhancement.

Denoising.

Prior traditional approaches to video denoising, such as those by Maggioni et al. (Maggioni et al. 2012) and Arias et al. (Arias and Morel 2018), are based on BM3D. Recent deep learning approaches, like those by Chen et al. (Chen, Song, and Yang 2016) and Qi et al. (Qi et al. 2022), have utilized CNNs for capturing temporal information. Qi et al. introduced a novel bidirectional buffer block in their BSVD framework (Qi et al. 2022).

Recent advancements include the work of Wang et al. (Wang et al. 2023), who extended text-driven generative models to long video generation with temporal co-denoising. Chan et al. (Chan et al. 2022) adapted the BasicVSR++ framework for video denoising, demonstrating the effectiveness of long-term propagation and alignment.

Yue et al. (Yue et al. 2020) introduced a novel dataset for dynamic scene video denoising with their RViDeNet. Tassano et al. (Tassano, Delon, and Veit 2020) presented FastDVD-net, notable for its real-time denoising capabilities. Finally, Claus and van Gemert (Claus and Van Gemert 2019) introduced ViDeNN, a CNN for blind video denoising, emphasizing the importance of specialized training data.

Joint Tasks.

There is some previous work on images for joint tasks of two. Zhou (Zhou, Li, and Loy 2022) proposed a CNN-based network for the joint task of low-light enhancement and deblurring on images, which uses Low-light enhancement encoder and deblurring decoder with filter skip connection. Zhao (Zhao et al. 2022) designed a two-stage method D2HNet for denoising and deblurring on images. Both methods produce their datasets for the joint tasks on image restoration.

For unifying the three tasks, Xu (Xu et al. 2022) proposed a kernel prediction network for the joint Video Super Resolution, low-light enhancement and denoising. They used both static and horizontal motion datasets.

Our Method

Overall Framework

In this work, we address the combined challenge of deblurring, enhancing low-light images, and denoising, framing it as a non-blind video restoration task. Utilizing synthetic datasets, we design a three-tiered decoder structure that progressively approaches different levels of ground truth. A feature fusion module links these tiers, facilitating the transition

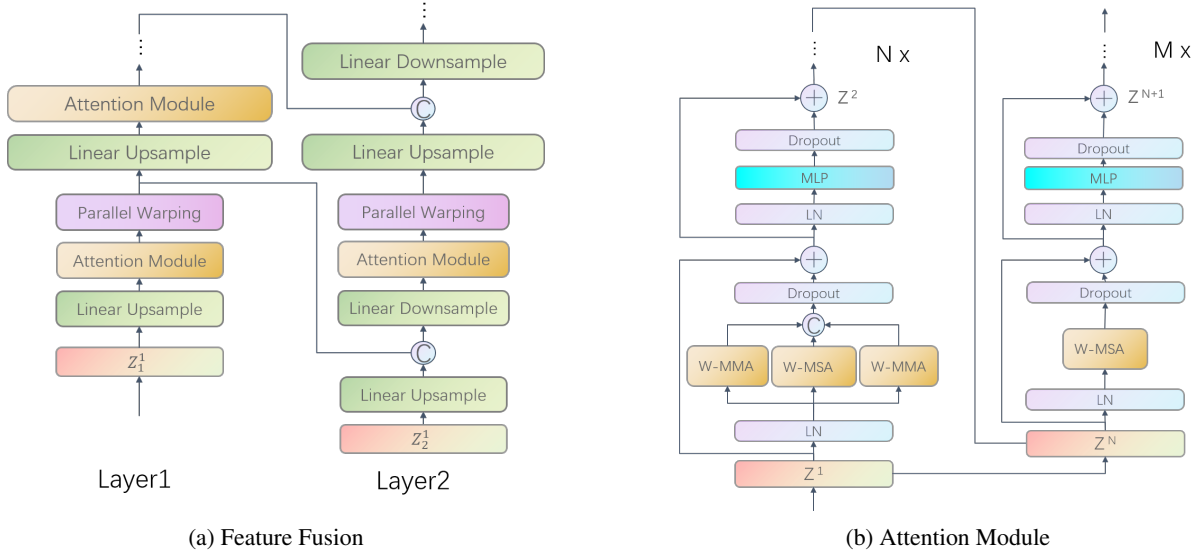


Figure 3: Illustrations for Feature Fusion between tiers and Attention Module in VJT. (a) shows the feature fusion between tier1 and tier2 at the first Attention-Warping module of the Decoder. (b) illustrates the attention module, which consists of N sub-parts containing W-MMA and M sub-parts with only W-MSA.

from shallow, singular feature learning to deep feature learning. To harmonize the three loss functions, we implement an adaptive weight scheme for more effective training.

Our Video Joint Task (VJT) framework aims to reconstruct high-quality frames from these low-quality inputs, I^{LQ} , which suffer from various degrees of video degradation. As illustrated in fig. 2, the VJT architecture comprises a shared Encoder and a Multi-tier Decoder.

Encoder

Our encoder features a multi-block pyramid structure, proven effective in feature clustering and parameter reduction in prior research.

Initially, spatial convolution extracts shallow features, yielding $Z^{Shallow}$. This is followed by a spatio-temporal attention module (detailed in fig. 3b and the Attention Module section). Next, we employ deformable convolution (Dai et al. 2017) to align adjacent frames, leveraging optical flow data from the Spynet framework (Ranjan and Black 2017). Finally, a downsample layer is passed. The above part is repeated three times to obtain the potential space Z^{Latent} .

Multi-tier Decoder

Our Multi-tier Decoder is architected as a tri-tier neural network, tailored to the complexity of the joint tasks it addresses. Each tier within this network is segmented into three distinct modules, scaled variably to handle different aspects of the processing pipeline. These modules are intricately composed of three fundamental operations: upsampling to enhance resolution, attention mechanisms to focus on salient

features, and warping to align and adjust frames temporally. Progressing beyond these initial operations, each tier sequentially integrates an additional four attention modules, further refining its focus and feature representation. This is followed by a reconstruction module, employing 3D convolutional layers for spatial-temporal data synthesis. The comprehensive design and structural intricacies of our Multi-tier Decoder are graphically delineated in fig. 2, elucidating its layered and modular approach in tackling complex video restoration tasks.

The output of the first tier, I_{DN}^R , is compared against the denoised target image I_{DN}^{GT} to compute the L_{DN} loss, aimed at enhancing the model’s capability to extract and refine denoised features effectively.

We have innovatively introduced a **Feature Fusion** module to synergize the capabilities of consecutive tiers. Taking the first two tiers as a case study, our objective is to amalgamate the latent features extracted from each module of the first tier into the subsequent tier. This process involves a strategic concatenation of the latent features Z_i^1 from the first tier with the preceding module’s output features Z_{i-1}^2 from the second tier. Subsequently, these combined features undergo downsampling, facilitated by layer normalization and linear transformation, to generate refined input features Z_i^2 for the next processing stage, as depicted in fig. 3a. This feature fusion concept is also applied between the twelve attention modules preceding the reconstruction phase, enhancing the overall feature integration and processing flow.

Attention Module

In our exploration of advanced Spatio-temporal attention mechanisms, we conducted a comprehensive analysis of existing methodologies and ultimately integrated the TMSA (Temporal Multi-head Self-Attention) framework from VRT (referenced in Liang et al., 2022). This choice was influenced by the framework’s innovative utilization of shifted window attention, a concept pioneered in the SwinTransformer (Liu et al., 2021).

The Attention module is architecturally composed of N parallel attention mechanisms and M window-based multi-head self-attentions (W-MSA). This dual-layered structure of attention is characterized by the integration of Window Mutual Multi-Head Attention (W-MMA), which operates between adjacent video frames, in conjunction with W-MSA. This unique arrangement enhances the module’s capacity to simultaneously process temporal dynamics and spatial details, as detailed in fig. 3b.

The parameter N is intrinsically tied to the number of video frames processed concurrently. Given that W-MMA facilitates mutual attention across pairs of frames, it becomes imperative that N is at least equivalent to the number of frames T being input, thereby ensuring comprehensive temporal coverage. Meanwhile, the M modules, primarily focused on W-MSA, are designed to recalibrate and intensify attention towards individual frame patches. Typically, M is calibrated to be between one-third and one-half of N , establishing a balanced attention distribution that prioritizes both inter-frame relationships and intra-frame details.

The Attention module uses the window mutual multi-head attention (WMMA) and window multi-head self-attention (WMSA) mechanisms to extract features. After that, it utilize MLP layers for dimensions reduction and feature fusion. The formula for the Attention module is as follows, Z_1 is the input and Z_2 is the output:

$$\begin{aligned}
 (X_1, X_2) &= LN(Z_1) \\
 Q_{1,2}, K_{1,2}, V_{1,2} &= MLP(X_{1,2}) \\
 \hat{Y}_1, \hat{Y}_2 &= WMMA(Q_{2,1}, K_{1,2}, V_{1,2}) \\
 Y_1, Y_2 &= WMSA(Q_{1,2}, K_{1,2}, V_{1,2}) \\
 \hat{Z}_1 &= MLP(Concatenate(\hat{Y}_1, \hat{Y}_2, Y_1, Y_2)) + Z_1 \\
 Z_2 &= MLP(LN(\hat{Z}_1)) + \hat{Z}_1
 \end{aligned} \tag{1}$$

Loss Function

In our multi-tier framework, we deploy triple set of loss functions, each tailored to a specific tier: L_{DN} for denoising, $L_{LE\&DN}$ for the combined low-light enhancement and denoising, and $L_{DB\&LE\&DN}$ for the integrated deblurring, illumination enhancement, and denoising. To ensure task coherence and uniform performance metrics across these tiers, we utilize the Charbonnier loss, a robust variant of the L1 norm, to measure the discrepancy between the output I_i^R ($i \in \{DN, LE\&DN, DB\&LE\&DN\}$) of each tier and its corresponding ground truth I_i^{GT} . The Charbonnier loss function is defined as follows:

$$\mathcal{L}_i(I_i^R, I_i^{GT}) = \sqrt{\|I_i^R - I_i^{GT}\|^2 + \epsilon} \tag{2}$$

where ϵ is a small positive constant that we set to 10^{-9} .

Given the multifaceted nature of our loss computation, encompassing diverse restoration tasks, we incorporate an **Adaptive Weighting Scheme** to dynamically balance the contribution of each individual loss function. This scheme draws inspiration from advanced multi-task learning strategies (Kendall, Gal, and Cipolla 2018) and is formulated by considering the multi-task likelihood as a composite of the individual task likelihoods. By applying logarithmic transformation aligned with the principles of maximum likelihood estimation, we obtain the following adaptive loss formulation:

In addressing the complexities of multi-task loss in our model, the challenge lies in optimally adjusting the weights of individual loss functions. To resolve this, we implement an **Adaptive Weighting Scheme**, grounded in established multi-task learning methodologies (Kendall, Gal, and Cipolla 2018). This approach conceptualizes the multi-task likelihood as the product of the likelihoods for each individual task. Through the application of a logarithmic transformation, consistent with maximum likelihood estimation principles, we derive an effective approximation:

$$\hat{\mathcal{L}}_i = \frac{1}{2\sigma_i^2} \mathcal{L}_i(I_i^R, I_i^{GT}) + \log \sigma_i \tag{3}$$

where σ_i denotes the model’s observation noise parameter of each tier. The Adam optimizer updates it to get better weights. Then, based on Liebel’s method (Liebel and Körner 2018), we modify the logarithmic form so that it would be stably convergent. Hence, we use:

$$\tilde{\mathcal{L}}_i = \frac{1}{2\sigma_i^2} \mathcal{L}_i(I_i^R, I_i^{GT}) + \log(1 + \sigma_i^2). \tag{4}$$

The overall loss function is:

$$\mathcal{L} = \tilde{\mathcal{L}}_{DN} + \tilde{\mathcal{L}}_{LE\&DN} + \tilde{\mathcal{L}}_{DB\&LE\&DN}. \tag{5}$$

It can adjust the weights faster to achieve better training results.

Our MLBN Dataset

A real lowlight-blur-noise dataset is difficult to collect because we cannot make the same random camera movements in the same scene, in normal light and low light. If we specify the camera motion pattern with a specific trace, the blur kernel is also determined, which does not work for the dataset. So we choose to generate our dataset. After systematic research, the existing low-light datasets, either under a fixed lens such as SMID dataset (Chen et al. 2019), or under a uniform horizontal movement such as SDDS dataset (Wang et al. 2021), were too simple in their motion to be suitable for our lowlight-blur-noise requirements. Our dataset is therefore intended to be generated based on the deblur dataset.

Our Multi-scenes Lowlight-Blur-Noise Dataset (MLBN Dataset) contains three main types of scenes: indoor scenes,

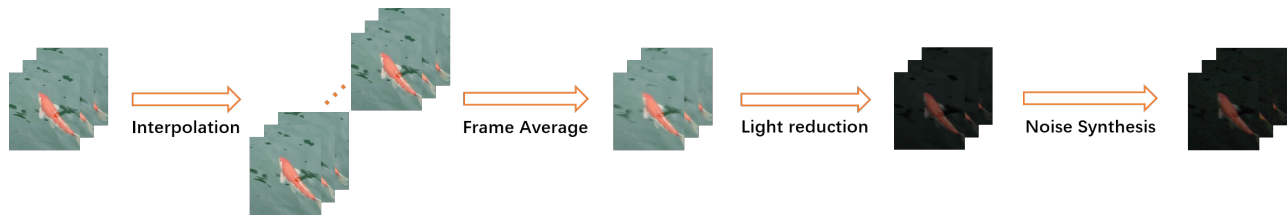


Figure 4: A concise diagram illustrates our data synthesis process.

nighttime outdoor scenes, and daytime outdoor scenes. The RealBlur dataset (Rim et al. 2020) is chosen as the basis for the indoor scenes and some of the night scenes. Besides, the day scenes and the other night scenes are generated from our own filming and 4K videos on YouTube. A total of 165 scenes containing 25 longer daytime outdoor videos are used for training, and another 30 scenes are used for testing.

Adding Motion Blur.

Firstly, in order to circumvent the relatively sharp blur caused by the averaging of a small number of frames, we initially employ the frame interpolation method RIFE to augment the original 60FPS video to 1920FPS, thereby ensuring the continuity of the blur. Then for 4k HD videos I_{4k}^{GT} , we resize them to 1280×720 I_{720}^{GT} . This step could effectively reduce the noise in videos. We centrally crop them to the same size as the RealBlur dataset for easy training and testing. After that, we perform the averaging process, ensuring the continuity of the blurriness. The most common method of generating blurry images is from the following blur model:

$$I^B = KI^{GT} + n \quad (6)$$

K is a large sparse matrix containing a local blur kernel at each row, and n is noise. However, since the inversion of K is ill-posed and not universal, we choose to generate the blurry image I^B based on method (Nah, Kim, and Lee 2016), using multi-frame temporal information:

$$I^B = g\left(\frac{1}{T} \sum_{t=1}^T g^{-1}(I_t^{GT})\right) \quad (7)$$

where g is the camera response function (CRF). Next, we take 10 seconds (total 19200 frames) of video from each scene, make a blurred image from 160 consecutive frames, and the middle frame is taken as the ground truth image so that these scenes will have 120 paired frames I^B & I^{GT} .

Reducing Illumination.

Starting with I^{Blur} , to be able to reduce illumination, we choose the Retinex model. Retinex theory is based on the central assumption that the image can be decomposed into the reflectance and the illumination components:

$$I^B = R \circ H \quad (8)$$

where I is the original image, R is the reflected component and H is the incident component, i.e. the illumination. Generally, H is enhanced to obtain a normally illuminated image.

We implement the inverse algorithm based on the Retinex method LIME (Guo, Li, and Ling 2016). After decomposing the normally illuminated image into R and H , H is weakened by gamma correction to obtain the new low-illumination map \hat{H} . In addition, unlike LIME, we also perform a slight attenuation of the R component to obtain \hat{R} , which is shown to produce an image that better matches the real scene in experiments. We obtain the low-light blur image as:

$$\hat{H} = H^{\gamma_1}, \hat{R} = R^{\gamma_2} \quad (9)$$

and

$$I^{L\&B} = \hat{R} \circ \hat{H}. \quad (10)$$

We also use the augmented Lagrangian multiplier (ALM) algorithm and possible weighting strategies to accelerate it.

Synthesise Noise.

Synthetic datasets are typically generated using the widely assumed additive white Gaussian noise (AWGN). However, they perform poorly when applied to real camera videos. This is mainly because AWGN is insufficient to model real camera noise, which is signal-dependent. Therefore, we adapt the CycleISP model that simulates a large number of transformations in a camera imaging pipeline for noise generation.

Experiments

Experiments Settings

We train all models with the learning rate initialized as $4e-4$ and adapted the cosine annealing schedule (Loshchilov and Hutter 2016) with a minimum learning rate of $1e-7$. We use the adam optimizer (Kingma and Ba 2014) for training with $\beta_1 = 0.9, \beta_2 = 0.99$ for a total of 100k iterations. In the adaptive weight scheme, we initialize all σ_i to 1. In addition, for the network, we use a pyramid structure with 3 downsample and upsample layers, followed by 4 equally sized attention modules.

Each input sequence has 6 frames, and the patch size is 192×192 , which is cropped in pairs randomly. Patches are also transformed by rotations of $90^\circ, 180^\circ, 270^\circ$ and horizontal flipping at random. And the window size of each patch is $6 \times 8 \times 8$.

In our model, we use a total of 7 layers of Attention-Warping modules of different scales and 4 layers of Attention modules of the same size. The latent channel numbers are 48, 60 respectively. For each of the 7 Attention-Warping modules, $N = 6$ layers with the window mutual multi-head

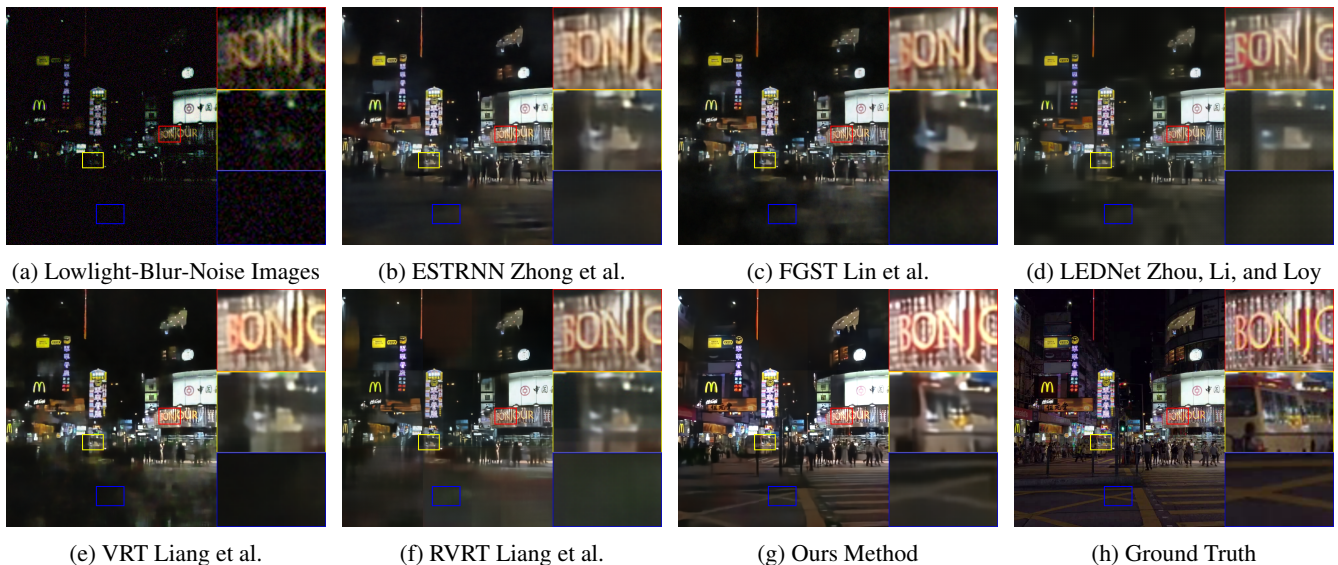


Figure 5: Qualitative visual comparisons on a frame of a night-time outdoor street scene in our MLBN dataset. Our approach demonstrates enhanced capabilities in restoring nighttime illumination, deblurring, and denoising. We mask it to show it more visually.

attention (WMMA) and window multi-head self-attention (WMSA) mechanism and $M = 2$ layers with only WMSA mechanism were used. Each of the 4 Attention modules contains 4 layers of WMSA mechanism module, for a total of 16 layers. The head numbers of multi-head attentions are all 6 and the deformable groups are 16. We also use DropPath in the model for better training.

We trained our model with batch size 4 on a server with 2 Intel Xeon Gold 6238R CPUs and 4 NVIDIA RTX A6000 GPUs. We adopt the PSNR and SSIM metrics for quantitative evaluation.

Evaluation on Our MLBN Dataset

Baselines. As there is no similar end-to-end method for the joint tasks of video deblurring, low-light enhancement and denoising before, we choose several state-of-the-art end-to-end models for video deblurring as our baselines. ESTRNN(Zhong et al. 2020) designed a global spatio-temporal attention module and used RDB-based RNN cells. FGST(Lin et al. 2022) proposed an optical flow-guided attention mechanism FGSW-MSA to expand the time-domain receptive field. LEDNet(Zhou, Li, and Loy 2022) designed a LE-Encoder for light enhancement and a Deblurring Decoder. VRT(Liang et al. 2022a) proposed neighbour frame attention and parallel warping with optical flow. The SOTA performance video transformer for deblurring is RVRT(Liang et al. 2022b), which propose a recurrent framework based on VRT. With their released code, these models are well-retrained on our Multi-scene-Lowlight-blur-noise (MLBN) dataset.

The comparative methods were trained until convergence, utilizing only the ground truth data from the final stage, due to their inherent structural configurations.

Table 1: Quantitative results with PSNR, SSIM metrics on our MLBN dataset. Videos with higher scores have better visual quality. The **BEST** results are in red, whereas the **SECOND BEST** ones are in blue. Our method achieves the best results on the MLBN dataset.

| Methods | PSNR \uparrow | SSIM \uparrow |
|---------------------------------|-----------------|-----------------|
| ESTRNN (Zhong et al. 2020) | 23.72 | 0.7600 |
| FGST (Lin et al. 2022) | 22.9434 | 0.6997 |
| LEDNet (Zhou, Li, and Loy 2022) | 23.98 | 0.7234 |
| VRT (Liang et al. 2022a) | 23.37 | 0.7430 |
| RVRT (Liang et al. 2022b) | 24.71 | 0.7612 |
| Ours | 25.45 | 0.8083 |

Quantitative Analysis. Table 1 shows the quantitative comparison results on the MLBN dataset. VJT achieves the best performance, outscoring the second-best method RVRT in terms of PSNR and SSIM by $0.74dB$ and 0.0471 . Compared to the joint image deblurring and illumination enhancement method LEDNet, we have even a $1.47dB$ improvement in PSNR. The total number of parameters of VJT is 12.17M, and the average running time of a frame is 692 ms. Because we have set the channel size(48,60) of our intermediate layer to half of VRT(96,120), although our framework appears large from the graph, in reality, both our encoder and each tier of decoder are less than half of VRT, and our total number of parameters is also smaller both than VRT and RVRT. More information about the model size and runtime of compared SOTA models can be found in Table 2.

Qualitative Analysis. Qualitative visual results for Joint Deblurring, Low-light Enhancement and Denoising on our MLBN dataset are shown in figs. 1 and 5. Overall, the results show that our method has two main advantages over other methods. Firstly, the results of our approach have more precise and sharper details, such as the ‘text board’ in fig. 1

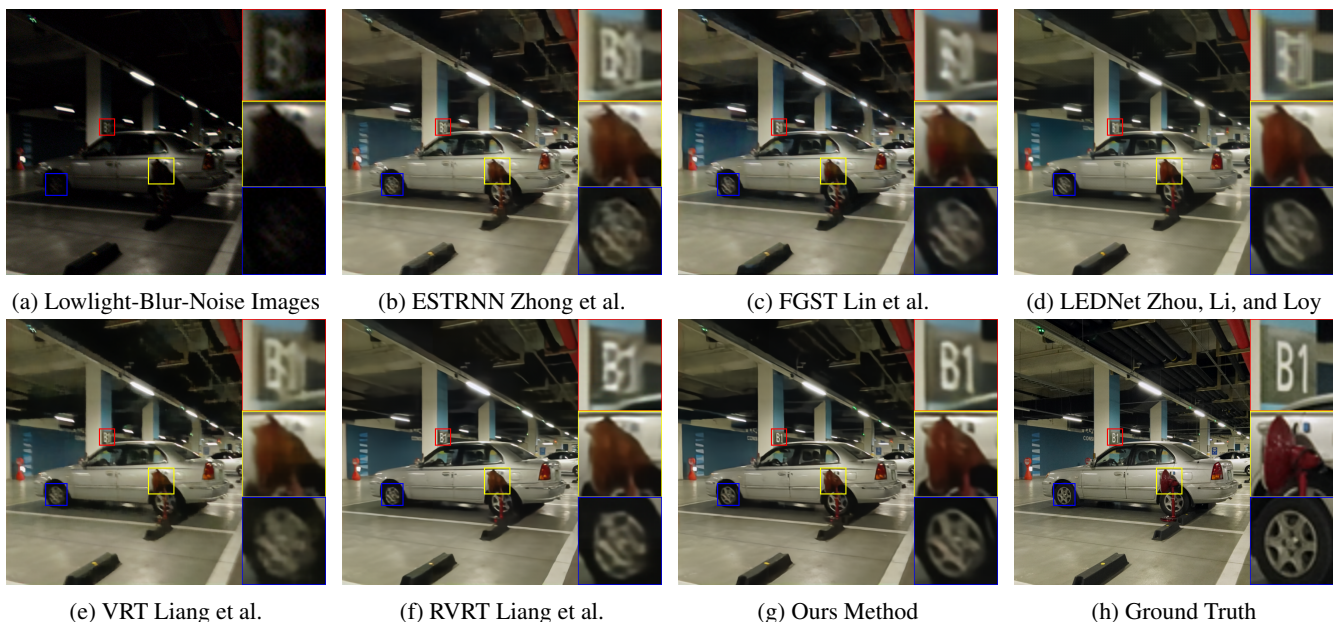


Figure 6: Qualitative visual comparisons on a frame of a indoor scene in our MLBN dataset. Our method offers improved **Deblurring and Denoising** effects, such as the 'B1' sign on the pillar, as well as enhanced illumination effects, like the red reflective mirror. We zoom in to show it more visually.

Table 2: Runtimes and model size between our methods and SOTA methods on 30 frames of a test scene, using an Intel(R) Xeon(R) Gold 6230 CPU and an NVIDIA Quadro RTX 8000 GPU.

| Methods | Avg.Time(ms) | Model Size(M) |
|---------|--------------|---------------|
| ESTRNN | 35 | 2.47 |
| FGST | 834 | 9.70 |
| LEDNet | 43 | 7.41 |
| VRT | 298 | 18.32 |
| RVRT | 442 | 13.57 |
| Ours | 692 | 12.17 |

and the "Shop logos on the street" in fig. 5. It shows that the frames processed with our method are more realistic than others. Second, blur in real-world videos often exhibits non-uniformity, with intensity varying between severe and mild blurring. fig. 5 illustrates that our approach outperforms other methods in scenarios characterized by uneven noise-induced blurring under low-light conditions. This holds true for light enhancement, denoising, and deblurring aspects.

As for real-world datasets, our model has been tested on the real-lol-blur dataset introduced by LEDNet, and the results are presented in Figure 8.

Compare to three stage concatenation methods

We employed a three-stage concatenation approach. For the Deblur stages, we utilized highly effective video methods, RVRT. As for the low-light enhancement phase, we employed the video method StableLLVE and image method Zerodce++ separately. And for the denoise stage, RVRT is also the SOTA method for video denoising. The results are in tables 3 and 4. We also compared different con-

catenation orders of Denoise, Deblur, and Lowligh Enhancement in table 4 by using RVRT-Deblur, StableLLVE-Lowligh Enhancement and RVRT-Denoise. On our dataset, we performed fine-tuning for both the RVRT model used for Deblur and Denoise tasks and the StableLLVE model utilized for low-light enhancement.

Within the progressive concatenation framework, the three distinct Ground Truths are derived from corresponding stages of different synthetic datasets, with the sequence of restoration tasks in the model mirroring the data generation sequence.

From the data presented in Tables 3 and 4, it is evident that our approach significantly outperforms the post-finetuning concatenation methods, achieving substantial leads in both PSNR and SSIM metrics. Additionally, we have verified that the order of concatenation in the methodology can lead to varying degrees of restoration effectiveness. The maximum difference observed in PSNR was approximately 1dB, and in SSIM, the maximum variation was up to 0.05.

In the concatenation experiments section of our comparative analysis, we indirectly demonstrated that there are discernible differences between varying sequences; The sequence we adopted in our model is aligned with the synthetic procedure of the dataset, which involves progressive Ground Truth data. This sequentiality is deliberate since video restoration serves as the inverse process to the methodical degradation encoded in the dataset generation.

Ablation Study

We present an ablation study to validate the effectiveness of the main components in VJT. Table 5 are the quantitative table of the ablation experiment.

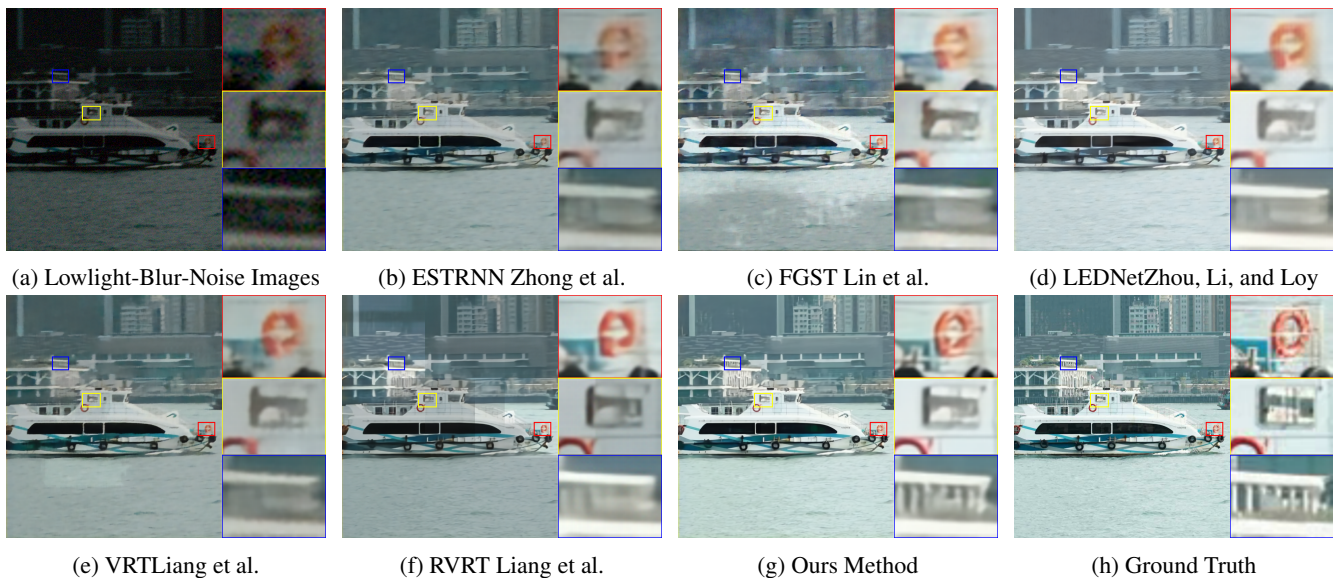


Figure 7: Qualitative visual comparisons on a frame of a daytime outdoor scene in our MLBN dataset. Our method delivers **Enhanced Illumination and Denoising** results, exemplified by the **lifebuoy on the bow of the boat**. We zoom in to show it more visually.

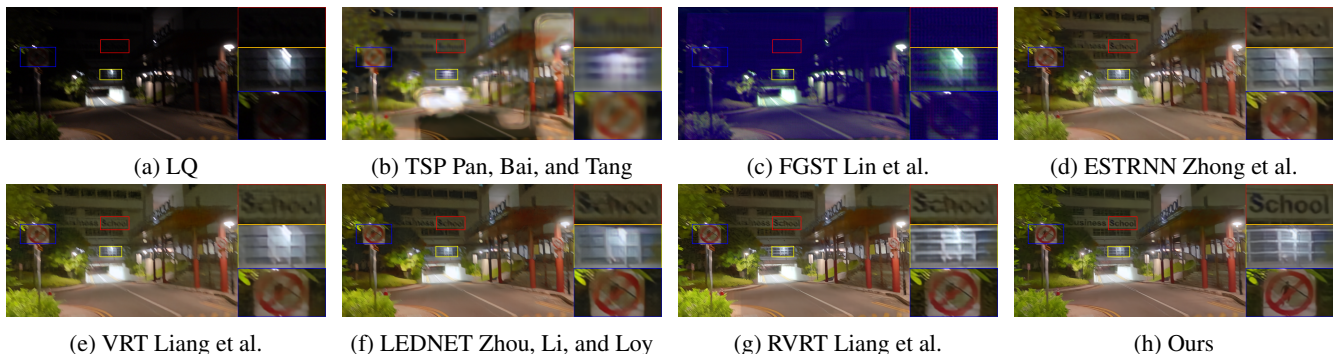


Figure 8: Experiment conducted on the real-lol-blur dataset provided by LEDNet. It can be observed that our method achieves sharper and brighter image restoration.

Table 3: Quantitative results compared with concatenation methods

| Deblur-LightEnhancement-Denoise | PSNR | SSIM |
|---------------------------------|--------------|---------------|
| RVRT-Zerodce+-RVRT | 14.90 | 0.2368 |
| RVRT-StableLLVE-RVRT | 16.75 | 0.3152 |
| Ours | 25.45 | 0.8083 |

Table 4: Different concatenation orders of Denoise, Deblur, and Lowligh Enhancement using retrained **RVRT-Denoise**, **StableLLVE-LowlighEnhancement** and **RVRT-Deblur**

| Methods | PSNR \uparrow | SSIM \uparrow |
|---------------------------------|-----------------|-----------------|
| Deblur-LightEnhancement-Denoise | 16.75 | 0.3152 |
| Deblur-Denoise-LightEnhancement | 17.087 | 0.315 |
| LightEnhancement-Deblur-Denoise | 16.04 | 0.2646 |
| LightEnhancement-Denoise-Deblur | 16.04 | 0.2649 |
| Denoise-Deblur-LightEnhancement | 17.002 | 0.3190 |
| Denoise-LightEnhancement-Deblur | 16.357 | 0.2685 |

Effectiveness of Multi-tier Architecture and Feature Fusion. The multi-tier framework and feature fusions are the foundation and core of our method, and removing them means VRT with channel size(48,60). Experiments show that our results are much higher than the VRT on PSNR and SSIM metrics.

Table 5: Ablation study on the MLBN dataset.

| Methods | PSNR \uparrow | SSIM \uparrow |
|-----------------------------|-----------------|-----------------|
| w/o multi-tier Architecture | 23.37 | 0.7430 |
| w/o Adaptive Weight Scheme | 24.71 | 0.7831 |
| Ours | 25.45 | 0.8083 |

Effectiveness of Adaptive Weight Scheme. During the training process, we observed that the ratio between the Losses becomes progressively smaller as the training converges. Simultaneously, the ratio of coefficients selected by the Adaptive Weight Scheme also diminishes, which shows that it can automatically adjust the energy levels of multiple

loss functions. The traditional grid method of setting coefficients, on the other hand, takes a lot of time to adjust the coefficients of the loss functions and often fails to find the best combination.

Conclusion

In this paper, we introduce a multi-tier video transformer (VJT) tailored for joint tasks of video deblurring, low-light enhancement, and denoising. Our VJT used videos with different degrees of degradation with multi-tier, and the feature fusion between tiers can learn features of the joint task progressively and gain better results. Moreover, we utilise adaptive weight loss for faster training, which can also improve model performance. Furthermore, we proposed a data generation progress and made a new Multi-scene Low-light Blur Noise (MLBN) dataset, which approximates various realistic scenes. Our network and dataset are both innovative and provide the basis of joint video tasks in the future. Experiments have clearly illustrated the leading performance of the proposed method. More results will be provided in the supplementary part. Dataset and Codes will be public.

References

- Abdullah-Al-Wadud, M.; Kabir, M. H.; Dewan, M. A. A.; and Chae, O. 2007. A dynamic histogram equalization for image contrast enhancement. *IEEE Transactions on Consumer Electronics*, 53(2): 593–600.
- Arias, P.; and Morel, J.-M. 2018. Video denoising via empirical Bayesian estimation of space-time patches. *Journal of Mathematical Imaging and Vision*, 60(1): 70–93.
- Arnab, A.; Dehghani, M.; Heigold, G.; Sun, C.; Lučić, M.; and Schmid, C. 2021. Vivit: A video vision transformer. In *Proceedings of the IEEE/CVF International Conference on Computer Vision*, 6836–6846.
- Bertasius, G.; Wang, H.; and Torresani, L. 2021. Is Space-Time Attention All You Need for Video Understanding? *Cornell University - arXiv, Cornell University - arXiv*.
- Carion, N.; Massa, F.; Synnaeve, G.; Usunier, N.; Kirillov, A.; and Zagoruyko, S. 2020. End-to-end object detection with transformers. In *European conference on computer vision*, 213–229. Springer.
- Chan, K. C.; Zhou, S.; Xu, X.; and Loy, C. C. 2022. On the generalization of basicvsr++ to video deblurring and denoising. *arXiv preprint arXiv:2204.05308*.
- Chen, C.; Chen, Q.; Do, M. N.; and Koltun, V. 2019. Seeing motion in the dark. In *Proceedings of the IEEE/CVF International Conference on Computer Vision*, 3185–3194.
- Chen, X.; Song, L.; and Yang, X. 2016. Deep rnns for video denoising. In *Applications of digital image processing XXXIX*, volume 9971, 573–582. SPIE.
- Claus, M.; and Van Gemert, J. 2019. Videnn: Deep blind video denoising. In *Proceedings of the IEEE/CVF conference on computer vision and pattern recognition workshops*, 0–0.
- Dai, J.; Qi, H.; Xiong, Y.; Li, Y.; Zhang, G.; Hu, H.; and Wei, Y. 2017. Deformable convolutional networks. In *Proceedings of the IEEE international conference on computer vision*, 764–773.
- Dosovitskiy, A.; Beyer, L.; Kolesnikov, A.; Weissenborn, D.; Zhai, X.; Unterthiner, T.; Dehghani, M.; Minderer, M.; Heigold, G.; Gelly, S.; Uszkoreit, J.; and Houlsby, N. 2021. An Image is Worth 16x16 Words: Transformers for Image Recognition at Scale. *ICLR*.
- Fu, X.; Liao, Y.; Zeng, D.; Huang, Y.; Zhang, X.-P.; and Ding, X. 2015. A probabilistic method for image enhancement with simultaneous illumination and reflectance estimation. *IEEE Transactions on Image Processing*, 24(12): 4965–4977.
- Girdhar, R.; Carreira, J.; Doersch, C.; and Zisserman, A. 2018. Video Action Transformer Network. *arXiv: Computer Vision and Pattern Recognition*.
- Gong, D.; Yang, J.; Liu, L.; Zhang, Y.; Reid, I.; Shen, C.; Van Den Hengel, A.; and Shi, Q. 2017. From motion blur to motion flow: A deep learning solution for removing heterogeneous motion blur. In *Proceedings of the IEEE conference on computer vision and pattern recognition*, 2319–2328.
- Guo, C.; Li, C.; Guo, J.; Loy, C. C.; Hou, J.; Kwong, S.; and Cong, R. 2020. Zero-reference deep curve estimation for low-light image enhancement. In *Proceedings of the IEEE/CVF Conference on Computer Vision and Pattern Recognition*, 1780–1789.
- Guo, X.; Li, Y.; and Ling, H. 2016. LIME: Low-light image enhancement via illumination map estimation. *IEEE Transactions on image processing*, 26(2): 982–993.
- Hao, P.; Wang, S.; Li, S.; and Yang, M. 2019. Low-light image enhancement based on retinex and saliency theories. In *2019 Chinese Automation Congress (CAC)*, 2594–2597. IEEE.
- Hyun Kim, T.; Mu Lee, K.; Scholkopf, B.; and Hirsch, M. 2017. Online video deblurring via dynamic temporal blending network. In *Proceedings of the IEEE international conference on computer vision*, 4038–4047.
- Ibrahim, H.; and Kong, N. S. P. 2007. Brightness preserving dynamic histogram equalization for image contrast enhancement. *IEEE Transactions on Consumer Electronics*, 53(4): 1752–1758.
- Ji, B.; and Yao, A. 2022. Multi-Scale Memory-Based Video Deblurring. In *Proceedings of the IEEE/CVF Conference on Computer Vision and Pattern Recognition*, 1919–1928.
- Kendall, A.; Gal, Y.; and Cipolla, R. 2018. Multi-task learning using uncertainty to weigh losses for scene geometry and semantics. In *Proceedings of the IEEE conference on computer vision and pattern recognition*, 7482–7491.
- Kim, T. H.; and Lee, K. M. 2015. Generalized video deblurring for dynamic scenes. *computer vision and pattern recognition*.
- Kingma, D. P.; and Ba, J. 2014. Adam: A method for stochastic optimization. *arXiv preprint arXiv:1412.6980*.
- Li, C.; Guo, J.; Porikli, F.; and Pang, Y. 2018a. LightenNet: A convolutional neural network for weakly illuminated image enhancement. *Pattern recognition letters*, 104: 15–22.

- Li, X.; Wu, J.; Lin, Z.; Liu, H.; and Zha, H. 2018b. Recurrent squeeze-and-excitation context aggregation net for single image deraining. In *Proceedings of the European conference on computer vision (ECCV)*, 254–269.
- Li, Y.; Kang, S. B.; Joshi, N.; Seitz, S.; and Huttenlocher, D. P. 2010. Generating sharp panoramas from motion-blurred videos. *computer vision and pattern recognition*.
- Liang, J.; Cao, J.; Fan, Y.; Zhang, K.; Ranjan, R.; Li, Y.; Timofte, R.; and Van Gool, L. 2022a. Vrt: A video restoration transformer. *arXiv preprint arXiv:2201.12288*.
- Liang, J.; Fan, Y.; Xiang, X.; Ranjan, R.; Ilg, E.; Green, S.; Cao, J.; Zhang, K.; Timofte, R.; and Van Gool, L. 2022b. Recurrent Video Restoration Transformer with Guided Deformable Attention. *arXiv preprint arXiv:2206.02146*.
- Liebel, L.; and Körner, M. 2018. Auxiliary tasks in multi-task learning. *arXiv preprint arXiv:1805.06334*.
- Lin, J.; Cai, Y.; Hu, X.; Wang, H.; Yan, Y.; Zou, X.; Ding, H.; Zhang, Y.; Timofte, R.; and Van Gool, L. 2022. Flow-Guided Sparse Transformer for Video Deblurring. *ICML*.
- Liu, Z.; Hu, H.; Lin, Y.; Yao, Z.; Xie, Z.; Wei, Y.; Ning, J.; Cao, Y.; Zhang, Z.; Dong, L.; Wei, F.; and Guo, B. 2022. Swin Transformer V2: Scaling Up Capacity and Resolution. In *International Conference on Computer Vision and Pattern Recognition (CVPR)*.
- Liu, Z.; Lin, Y.; Cao, Y.; Hu, H.; Wei, Y.; Zhang, Z.; Lin, S.; and Guo, B. 2021a. Swin transformer: Hierarchical vision transformer using shifted windows. In *Proceedings of the IEEE/CVF International Conference on Computer Vision*, 10012–10022.
- Liu, Z.; Ning, J.; Cao, Y.; Wei, Y.; Zhang, Z.; Lin, S.; and Hu, H. 2021b. Video Swin Transformer. *arXiv preprint arXiv:2106.13230*.
- Lore, K. G.; Akintayo, A.; and Sarkar, S. 2017. LLNet: A deep autoencoder approach to natural low-light image enhancement. *Pattern Recognition*, 61: 650–662.
- Loshchilov, I.; and Hutter, F. 2016. Sgdr: Stochastic gradient descent with warm restarts. *arXiv preprint arXiv:1608.03983*.
- Lv, F.; Lu, F.; Wu, J.; and Lim, C. 2018. MBLLEN: Low-Light Image/Video Enhancement Using CNNs. *British Machine Vision Conference, British Machine Vision Conference*.
- Maggioni, M.; Boracchi, G.; Foi, A.; and Egiazarian, K. 2012. Video denoising, deblocking, and enhancement through separable 4-D nonlocal spatiotemporal transforms. *IEEE Transactions on image processing*, 21(9): 3952–3966.
- Nah, S.; Kim, T. H.; and Lee, K. M. 2016. Deep Multi-scale Convolutional Neural Network for Dynamic Scene Deblurring. *computer vision and pattern recognition*.
- Pan, J.; Bai, H.; and Tang, J. 2020. Cascaded Deep Video Deblurring Using Temporal Sharpness Prior. In *IEEE/CVF Conference on Computer Vision and Pattern Recognition (CVPR)*.
- Park, S.; Yu, S.; Moon, B.; Ko, S.; and Paik, J. 2017. Low-light image enhancement using variational optimization-based retinex model. *IEEE Transactions on Consumer Electronics*, 63(2): 178–184.
- Peng, B.; Zhang, X.; Lei, J.; Zhang, Z.; Ling, N.; and Huang, Q. 2022. LVE-S2D: Low-light video enhancement from static to dynamic. *IEEE Transactions on Circuits and Systems for Video Technology*.
- Qi, C.; Chen, J.; Yang, X.; and Chen, Q. 2022. Real-time Streaming Video Denoising with Bidirectional Buffers. In *Proceedings of the 30th ACM International Conference on Multimedia*, 2758–2766.
- Ranjan, A.; and Black, M. J. 2017. Optical flow estimation using a spatial pyramid network. In *Proceedings of the IEEE conference on computer vision and pattern recognition*, 4161–4170.
- Rim, J.; Lee, H.; Won, J.; and Cho, S. 2020. *Real-World Blur Dataset for Learning and Benchmarking Deblurring Algorithms*, 184–201.
- Son, H.; Lee, J.; Lee, J.; Cho, S.; and Lee, S. 2021. Recurrent video deblurring with blur-invariant motion estimation and pixel volumes. *ACM Transactions on Graphics (TOG)*, 40(5): 1–18.
- Su, S.; Delbraccio, M.; Wang, J.; Sapiro, G.; Heidrich, W.; and Wang, O. 2017. Deep video deblurring for hand-held cameras. In *Proceedings of the IEEE conference on computer vision and pattern recognition*, 1279–1288.
- Tassano, M.; Delon, J.; and Veit, T. 2019. Dvdnet: A fast network for deep video denoising. In *2019 IEEE International Conference on Image Processing (ICIP)*, 1805–1809. IEEE.
- Tassano, M.; Delon, J.; and Veit, T. 2020. Fastdvdnet: Towards real-time deep video denoising without flow estimation. In *Proceedings of the IEEE/CVF conference on computer vision and pattern recognition*, 1354–1363.
- Triantafyllidou, D.; Moran, S.; McDonagh, S.; Parisot, S.; and Slabaugh, G. 2020. Low light video enhancement using synthetic data produced with an intermediate domain mapping. In *European Conference on Computer Vision*, 103–119. Springer.
- Vaswani, A.; Shazeer, N.; Parmar, N.; Uszkoreit, J.; Jones, L.; Gomez, A. N.; Kaiser, Ł.; and Polosukhin, I. 2017. Attention is all you need. *Advances in neural information processing systems*, 30.
- Wang, F.-Y.; Chen, W.; Song, G.; Ye, H.-J.; Liu, Y.; and Li, H. 2023. Gen-L-Video: Multi-Text to Long Video Generation via Temporal Co-Denoising. *arXiv preprint arXiv:2305.18264*.
- Wang, R.; Xu, X.; Fu, C.-W.; Lu, J.; Yu, B.; and Jia, J. 2021. Seeing Dynamic Scene in the Dark: A High-Quality Video Dataset with Mechatronic Alignment. In *Proceedings of the IEEE/CVF International Conference on Computer Vision*, 9700–9709.
- Wang, R.; Zhang, Q.; Fu, C.-W.; Shen, X.; Zheng, W.-S.; and Jia, J. 2019a. Underexposed photo enhancement using deep illumination estimation. In *Proceedings of the IEEE/CVF Conference on Computer Vision and Pattern Recognition*, 6849–6857.
- Wang, T.; Yang, X.; Xu, K.; Chen, S.; Zhang, Q.; and Lau, R. W. 2019b. Spatial attentive single-image deraining with a high quality real rain dataset. In *Proceedings of*

- the *IEEE/CVF Conference on Computer Vision and Pattern Recognition*, 12270–12279.
- Wang, X.; Chan, K. C.; Yu, K.; Dong, C.; and Change Loy, C. 2019c. Edvr: Video restoration with enhanced deformable convolutional networks. In *Proceedings of the IEEE/CVF Conference on Computer Vision and Pattern Recognition Workshops*, 0–0.
- Wei, C.; Wang, W.; Yang, W.; and Liu, J. 2018. Deep retinex decomposition for low-light enhancement. *arXiv preprint arXiv:1808.04560*.
- Wulff, J.; and Black, M. J. 2014. Modeling Blurred Video with Layers. *European conference on computer vision*.
- Xie, Z.; Lin, Y.; Yao, Z.; Zhang, Z.; Dai, Q.; Cao, Y.; and Hu, H. 2021. Self-Supervised Learning with Swin Transformers. *arXiv preprint arXiv:2105.04553*.
- Xu, K.; Yang, X.; Yin, B.; and Lau, R. W. 2020. Learning to restore low-light images via decomposition-and-enhancement. In *Proceedings of the IEEE/CVF Conference on Computer Vision and Pattern Recognition*, 2281–2290.
- Xu, X.; Wang, R.; Fu, C.-W.; and Jia, J. 2022. Deep Parametric 3D Filters for Joint Video Denoising and Illumination Enhancement in Video Super Resolution. *arXiv preprint arXiv:2207.01797*.
- Yang, W.; Liu, J.; and Feng, J. 2019. Frame-consistent recurrent video deraining with dual-level flow. In *Proceedings of the IEEE/CVF Conference on Computer Vision and Pattern Recognition*, 1661–1670.
- Yang, W.; Wang, W.; Huang, H.; Wang, S.; and Liu, J. 2021. Sparse gradient regularized deep retinex network for robust low-light image enhancement. *IEEE Transactions on Image Processing*, 30: 2072–2086.
- Yue, H.; Cao, C.; Liao, L.; Chu, R.; and Yang, J. 2020. Supervised raw video denoising with a benchmark dataset on dynamic scenes. In *Proceedings of the IEEE/CVF conference on computer vision and pattern recognition*, 2301–2310.
- Yue, Z.; Xie, J.; Zhao, Q.; and Meng, D. 2021. Semi-supervised video deraining with dynamical rain generator. In *Proceedings of the IEEE/CVF Conference on Computer Vision and Pattern Recognition*, 642–652.
- Zhang, F.; Li, Y.; You, S.; and Fu, Y. 2021. Learning temporal consistency for low light video enhancement from single images. In *Proceedings of the IEEE/CVF Conference on Computer Vision and Pattern Recognition*, 4967–4976.
- Zhang, H.; Xie, H.; and Yao, H. 2022. Spatio-Temporal Deformable Attention Network for Video Deblurring. In *European Conference on Computer Vision*, 581–596. Springer.
- Zhang, K.; Li, D.; Luo, W.; Ren, W.; and Liu, W. 2022. Enhanced spatio-temporal interaction learning for video deraining: A faster and better framework. *IEEE Transactions on Pattern Analysis and Machine Intelligence*.
- Zhang, Y.; Zhang, J.; and Guo, X. 2019. Kindling the darkness: A practical low-light image enhancer. In *Proceedings of the 27th ACM international conference on multimedia*, 1632–1640.
- Zhao, Y.; Xu, Y.; Yan, Q.; Yang, D.; Wang, X.; and Po, L.-M. 2022. D2HNet: Joint Denoising and Deblurring with Hierarchical Network for Robust Night Image Restoration. *arXiv preprint arXiv:2207.03294*.
- Zhong, Z.; Gao, Y.; Zheng, Y.; and Zheng, B. 2020. Efficient spatio-temporal recurrent neural network for video deblurring. In *European Conference on Computer Vision*, 191–207. Springer.
- Zhong, Z.; Zheng, Y.; and Sato, I. 2021. Towards rolling shutter correction and deblurring in dynamic scenes. In *Proceedings of the IEEE/CVF Conference on Computer Vision and Pattern Recognition*, 9219–9228.
- Zhou, S.; Li, C.; and Loy, C. C. 2022. LEDNet: Joint Low-light Enhancement and Deblurring in the Dark. In *ECCV*.